TEMPLATE METHOD TO IMPROVE BRAIN SEGMENTATION FROM INHOMOGENEOUS BRAIN MAGNETIC RESONANCE IMAGES AT HIGH FIELDS

Marcelo A. Castro[1], Jianhua Yao[1], Yuxi Pang[1,2], Eva Baker[1], John Butman[1], David Thomasson[1]

[1] National Institutes of Health – Department of Radiology and Imaging Sciences
[2] Philips Healthcare

ABSTRACT

Magnetic resonance imaging of the brain at high fields (e.g. 3T) provides high resolution and high signal to noise ratio images suitable for a wide range of clinical applications. However, radiofrequency (or B_1) inhomogeneity increases with the magnetic field and produces undesired intensity variations responsible for inaccuracies in quantitative analyses. A method to perform brain segmentation using T_1 maps whose inhomogeneity was corrected using previously acquired B_1 maps is described. A library of B_1 maps was created and a method to compensate the T_1 inhomogeneity using a B_1 map from another subject (template) was developed. The performance of the template-based method was evaluated in 19 healthy volunteers. Our method produced significantly better segmentations than the retrospective N3 method and the one without B_1 inhomogeneity correction.

Index Terms— Magnetic resonance imaging, Image registration, Image segmentation, Brain.

1. INTRODUCTION

Accurate segmentation of MR brains images is of interest in the study of pathologies such as schizophrenia, epilepsy, multiple sclerosis and Alzheimer's disease where volumetric analysis of gray matter (GM), white matter (WM) and cerebrospinal fluid (CSF) is needed [1], [2]. Most segmentation methods can be grouped in three major classes: contour-based, region-based, and classification-based methods [3].

Contour-based methods segment the regions by detecting their boundaries using gradients [4] or active contours [5], [6]. Those based on edge detection are sensitive to noise and artifacts, and sophisticated processing is needed to achieve a satisfactory segmentation. Active contours methods have difficulty with typical non smooth boundaries in brains [3].

Region-based methods identify the various homogeneous regions that correspond to different tissues by considering spatial interaction between neighboring pixels [3], [7].

In classification-based segmentation, pixels are labeled as belonging to a particular tissue class according to a certain criterion. The simplest technique is based on thresholding [8]. However, this approach is sensitive to inhomogeneities. This limitation is addressed by statistical classification methods, where the probability density function is often modeled parametrically as a mixture of Gaussians [9]. The most popular unsupervised classification methods are the clustering-based methods. Clustering algorithms classify a voxel to a tissue class by using the notion of similarity [10]. A modified fuzzy c-means algorithm that corrects the inhomogeneity during the clustering process by modeling the inhomogeneity field was presented [3].

Brain segmentation can also be performed from T_1 maps. The variable flip angle method, which is widely used to produce T_1 maps in a reasonable time frame, is based on acquiring spoiled gradient recalled-echo (SPGR) images with various different flip angles with the repetition time (T_R) held constant. According to Wang et al., for any given T_R/T_1 ratio, there exist two optimal flip angles that minimize the uncertainty in the estimated T_1 values [11]. Proper T_1 estimation requires minimizing the effects of spatial variations of the transmitted flip angle, which is proportional to the prescribed angle α according to the spatial variation of the B_1 field [12]. This effect is more prominent at high magnetic fields needed to increase the signal-to-noise ratio [13]. A joint brain parametric T_1-map segmentation and radiofrequency inhomogeneity calibration has been recently presented [14] where the inhomogeneity is corrected based on the assumption that the mean T_1 of WM is the same across the central brain slices. Inhomogeneity can be corrected retrospectively (e.g. by estimating the multiplicative inhomogeneity field and the additive noise distribution) or prospectively (e.g. by acquiring additional data) [15].

Many retrospective methods can be found in the literature [15], [16]. A particular approach proposed by Sled et al. is the N3 method [17], which derives a non-parametric model of the tissue intensity directly from the data. The N3 method does not require a model of the tissue intensities in terms of discrete tissue classes, nor does it rely on a segmentation of the volume into homogeneous regions. The method assumes that the mean intensity is preserved. The method finds the smooth, slowly varying multiplicative field that maximizes the frequency content of the distribution of tissue intensities.

Different prospective methods to compensate B_1 field inhomogeneity by acquiring additional images have been presented in the past. Ishimori et al. proposed a method to estimate and correct B_1 inhomogeneity that uses multiple spoiled gradient recalled-echo (SPGR) images for 3T MRI, which relied on the acquisition of several images with different echo times (T_E) and flip angles for a fixed T_R [18]. Treier et al. presented a combined T_1 and B_1 mapping technique for T_1 estimation in abdominal contrast-enhanced MRI [19] that computes T_1 maps from two T_1w images acquired using two optimal flip angles [11] and compensates the B_1 inhomogeneity using a subject-specific B_1 map acquired by means of a dual T_R method [20]. Deoni presented a method that combines the usual multi-angle SPGR data with one inversion-prepared SPGR data to obtain a unique solution for the T_1 map, the factor proportional to the longitudinal magnetization and the spatial variation of the radiofrequency field [21].

In the clinical setting, it is beneficial to minimize scanning time and it would be desirable that B_1 corrections may be made from a

template, obviating the need for obtaining a B_1 map each and every time a patient is scanned. Using template B_1 maps would also allow more accurate quantitative analyses in studies where B_1 maps were not previously acquired. A set of template B_1 maps can be used to improve the performance of the correction method.

Our template-based B_1 correction method is based on Treier's technique with the incorporation of modules to align images and to transform B_1 maps from other subjects. We investigated the shift in the mean value of the corrected T_1 map when compared to the non-corrected one also reported by Treier [19], which is in disagreement with the assumption that the mean intensity is preserved, used in retrospective methods like the N3 method. B_1 inhomogeneity in brain T_1 maps computed from registered images was compensated using the B_1 maps from the same and all the other subjects. B_1 maps were previously registered and the performance of the correction was evaluated. The T_1 values and the brain segmentation were studied to compare the quality of the template-based and the N3 corrections.

2. METHODS

2.1. Subjects and imaging

Nineteen normal volunteers (9 males and 10 females) with ages between 23 and 62 (mean ± stdev = 39.1 ± 11.3) without history of neurological diseases were considered in this study. The imaging protocol was approved by the institutional review board and informed consent was obtained from all subjects. Imaging was performed using a 3T Philips system (Philips, Best, NL) equipped with Explorer gradients using a SENSE head coil. Two 3D T_1w fast field echo (FFE) images (48 slices, FOV=240mm x 240mm, slice thickness= 3.0mm, matrix= 480x480) in an axial orientation were acquired using a dual flip angle SPGR protocol ($T_R/T_E/FA_1/FA_2$ = 6ms/2.3ms/5deg/15deg), with flip angles selected to achieve maximum accuracy in the range of WM and GM [19]. Another two T_1w images (24 slices, FOV= 240 mm x 240 mm, slice thickness= 6.0 mm, matrix= 240x240) were acquired to produce B_1 maps from a dual-T_R SPGR protocol ($T_{R1}/T_{R2}/FA/T_E$ = 50ms/ 250ms/60deg/5ms). T_R was chosen based on the optimum ratio in the range of 4-6 in order for the ratio between signal intensities to be sensitive to flip angle variations, with $T_{R1}<T_{R2}<T_1$ [20]. The total acquisition time is 7:30 min.

2.2. T_1 mapping with B_1 inhomogeneity corrected

The variable flip angle method for T_1 estimation uses consecutively acquired T_1w SPGR (T_1-FFE) images with different flip angles. Images were aligned using a six-parameter rigid registration with a mutual information metric and linear interpolation using 64 histogram bins and the number of spatial samples equal to 1% of the image pixels [22]. T_1 maps were generated from two optimal flip angles [21]. Each image has a theoretical signal intensity S that depends on the prescribed flip angle α, the magnetization M_0, the relaxation times T_1 and T_2, the echo time T_E, and the repetition time T_R (1). That intensity can also be written as a linear relation between $S/\sin(\alpha)$ and $S/\tan(\alpha)$ (2), where $\exp(-T_E/T_2) \approx 1$ since T_E = 2.3 ms and T_2 for WM and GM tissues at 3T ranges between 50 and 100 ms [19], [23]. The slope m in (2) can be obtained and used to compute T_1 (3) at every pixel, from S_1 and S_2 corresponding to flip angles α_1 and α_2.

$$S = M_0 \frac{\sin(\alpha)\left(1 - e^{-\frac{T_R}{T_1}}\right)e^{-\frac{T_E}{T_2}}}{1 - e^{-\frac{T_R}{T_1}}\cos(\alpha)}. \quad (1)$$

$$\left(\frac{S}{\sin(\alpha)}\right) = e^{-\frac{T_R}{T_1}}\left(\frac{S}{\tan(\alpha)}\right) + M_0\left(1 - e^{-\frac{T_R}{T_1}}\right)e^{-\frac{T_E}{T_2}}. \quad (2)$$

$$m = \frac{\frac{S_1}{\sin(\alpha_1)} - \frac{S_2}{\sin(\alpha_2)}}{\frac{S_1}{\tan(\alpha_1)} - \frac{S_2}{\tan(\alpha_2)}} \quad ; \quad T_1 = -\frac{T_R}{\ln(m)} \quad (3)$$

B_1 maps are generated from a dual T_R technique. Two images are acquired with different T_R but the same T_E and α [20]. Maps are tri-linearly interpolated to obtain B_1 inhomogeneity values at the image nodes. Since B_1 maps provide a distribution of correction factors (ranging between 0.50 and 1.50) for the ideally uniform prescribed flip angle, the corrected slope m_{corr} is used to compute the corrected T_1 values (T_1^{corr}) at every voxel [19] given by (4).

$$m_{corr} = \frac{\frac{S_1}{\sin(B_1\alpha_1)} - \frac{S_2}{\sin(B_1\alpha_2)}}{\frac{S_1}{\tan(B_1\alpha_1)} - \frac{S_2}{\tan(B_1\alpha_2)}} \quad ; \quad T_1^{corr} = -\frac{T_R}{\ln(m_{corr})} \quad (4)$$

The non-linear relation between T_1^{corr} and B_1 in (4) produces higher shifts towards higher T_1 values when $B_1<1$ than those towards lower T_1 values when $B_1>1$ for typical S_1 and S_2. Thus, if the average B_1 in the map is less than 1, the averaged T_1^{corr} will be higher than the uncorrected one.

2.2. Template-based B_1 correction

In order to minimize scanning time and allow more accurate quantitative analyses in studies where B_1 maps were not previously acquired, it would be desirable that avoid B_1 map acquisition every time a new patient is scanned. This problem may be solved either by using templates or by retrospective methods.

For the template based B_1 correction, we first build a library of B_1 maps acquired by the dual-T_R method. Then, given a new study i, we examine it against every study j (templates) in the library in the following way. First, the T_1w images from study i and template j (T_1w^i and T_1w^j) are aligned using a 12-parameter affine registration with mutual information metric and linear interpolation using 64 histogram bins and the number of spatial samples equal to 1% of the image pixels. Afterwards, the B_1 map of template j (B_1^j) is aligned according to that transformation in order to match the geometry of the subject under study i. The transformed B_1 map is used to compute the template correction. The best template-corrected map (T_1^{tem}) is found as the one that maximizes the pixel intensity agreement factor (5) in T_1 values when compared to the reference T_1 map (T_1^{ref}), which is the T_1 map corrected using the same subject B_1 map.

For the retrospective approach, a MIPAV implementation of the N3 method (http://mipav.cit.nih.gov) was applied to both T_1w

images to remove the inhomogeneity. Those images were used to generate a corrected map (T_1^{N3}) in the same way as it was described before. It is expected that a T_1 map generated from retrospectively corrected images should be comparable to a T_1 map prospectively corrected using subject-specific or a template-based B_1 map. However, since the N3 method, like many other retrospective correction methods, assumes that the mean T_1 value of the brain is preserved, not necessarily true according to Section 2.2, different correction approaches must be compared.

The brains were extracted from T_1^{ref} using a brain extraction tool that uses a deformable model that evolves to fit the brain surface by the application of a set of locally adapted forces [24]. The brain mask was then applied in T_1^{tem} and T_1^{N3}, and the uncorrected map (T_1^{nc}). In this way, possible inaccuracies in the extraction of the brain from inhomogeneous images are minimized [24].

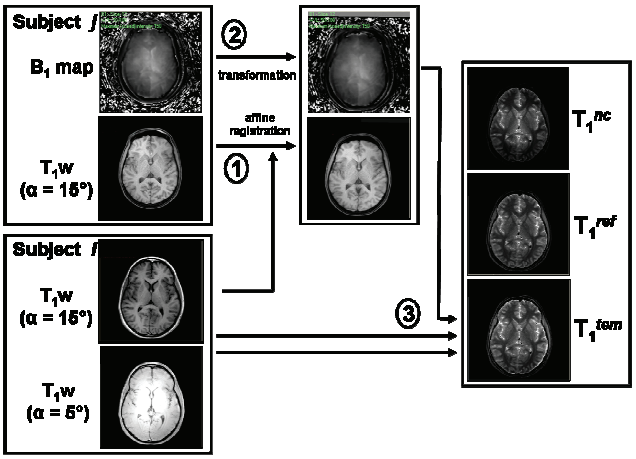

Fig. 1. Methodology to generate a corrected T_1 map of Subject *i* using B_1^j. (1) High-flip-angle T_1w^i and T_1w^i images are aligned. (2) The transformation is applied to the B_1^j. (3) T_1w images of Subject *i* and the B_1^j are used to generate T_1^{tem}.

2.3. Data analysis: T_1 calculation and T_1 map segmentation

The pixel intensity agreement factor (P_1) between T_1^{ref} and T_1^{nc}, T_1^{N3} and T_1^{tem} was computed, called as P_1^{nc}, P_1^{N3} and P_1^{tem} respectively, and N is the number of pixels in the brain (5). Additionally, all T_1 maps were segmented in four classes (background, WM, GM and CSF) using the MIPAV implementation (http://mipav.cit.nih.gov) of the fuzzy c-means algorithm. The segmentation accuracy factor (P_2), which is defined as the number of pixels classified in the same category as in T_1^{ref} (N_{WM}^{WM}, N_{GM}^{GM} and N_{CSF}^{CSF}) divided by N (6) is computed and used to characterize the performance of the correction method. The P_2 values for the same subjects are called P_2^{nc}, P_2^{N3} and P_2^{tem}. A hypothesis t-test for unequal variances is performed to characterize the improvement of P_1^{tem} with respect to P_2^{N3} and P_1^{nc}, and of P_2^{tem} with respect to P_2^{N3} and P_2^{nc}.

$$P_1 = \frac{1}{N}\sum_{i,j,k\in brain}^{N} \frac{\left|T_1(i,j,k) - T_1^{ref}(i,j,k)\right|}{T_1^{ref}(i,j,k)}, \quad (i,j,k)\in brain \qquad (5)$$

$$P_2 = \frac{N_{WM}^{WM} + N_{GM}^{GM} + N_{CSF}^{CSF}}{N} \qquad (6)$$

3. RESULTS

B_1 maps contain correction factors for the actual flip angle (0.50 to 1.50). Mean B_1 values ranged between 0.85 and 0.96 (average±stdev = 0.89±0.03). Therefore, based on (4), higher T_1 values are expected in T_1^{ref} compared to T_1^{nc} and T_1^{N3}. It was also observed that T_1^{nc} with large mean values are better corrected (larger P_1) by a template B_1 maps with a T_1^{nc} map whose mean value is also large.

Fig. 2 shows the T_1 maps (left) and segmentations (right) for T_1^{ref} (a,b), T_1^{tem} (c,d), T_1^{N3} (e,f), and T_1^{nc} (g,h). It was observed that the inhomogeneity affects the segmentation (Fig. 2g,h). The segmentation after N3 correction (Fig. 2f) differ from the reference one (Fig. 2b), while the use of the best template (Fig. 2d) results in similar segmentations.

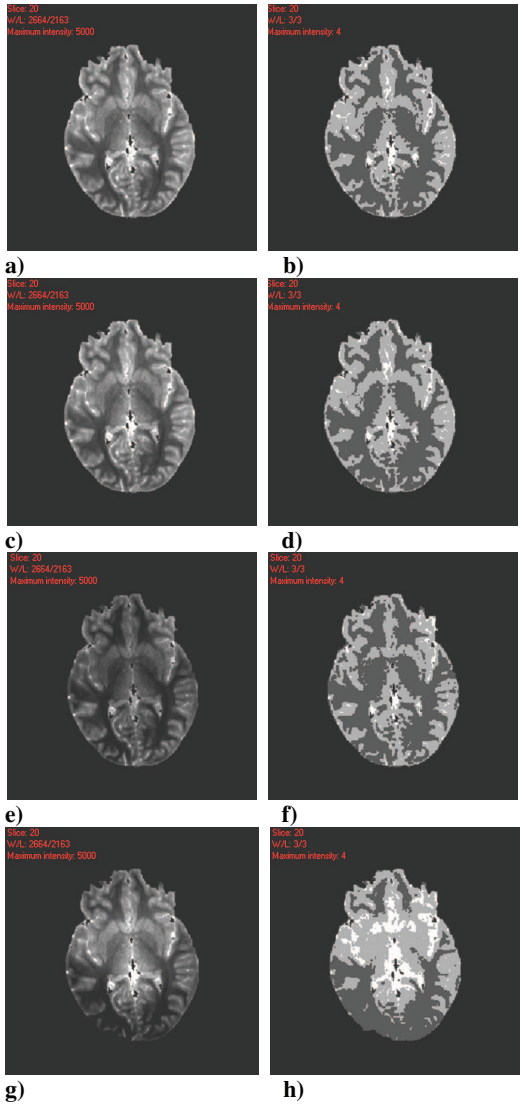

Fig. 2. T_1 maps (a,c,e,g) and segmentations (b,d,f,h) for selected Subject #14. a,b) T_1^{ref}; c,d) T_1^{tem}; e,f) T_1^{N3}; g,h) T_1^{nc}. Intensity in segmented maps correspond to T_1 values: background (black); WM (dark gray); GM (light gray); CSF (white).

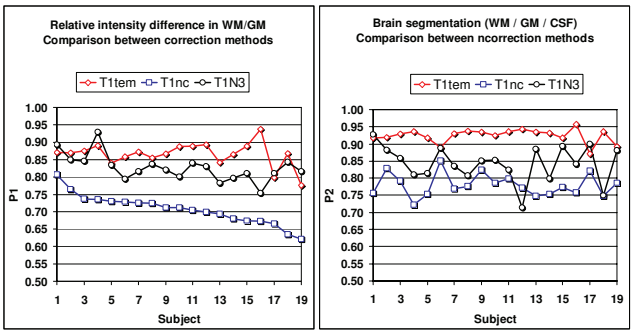

a) **b)**

Fig. 3. a) Relative difference in intensity in WM and GM regions for T_1^{nc}, T_1^{tem} and T_1^{N3}, compared to T_1^{ref}; b) Similarity between brain segmentations of T_1^{ref}, and T_1^{nc}, T_1^{tem} and T_1^{N3}.

A hypothesis tests showed that both P_1 and P_2 for T_1^{tem} are significantly higher (p-value < 0.001) than those for T_1^{N3} and T_1^{nc}. (see Table 1. The N3 method preserves the mean value of the uncorrected map therefore, P_1^{N3} is smaller than P_1^{tem}. The data for all subjects is shown in Figures 3a,b.

	P_1^{tem}	P_1^{N3}	P_1^{nc}	P_2^{tem}	P_2^{N3}	P_2^{nc}
mean	0.87	0.83	0.71	0.92	0.84	0.78
stdev	0.04	0.04	0.04	0.02	0.05	0.03

Table 1. Mean value and standard deviation for the pixel intensity agreement and segmentation accuracy factors in T_1^{tem},$T_1^{N3}$and T_1^{nc}.

4. CONCLUSIONS

The B_1 inhomogeneity correction method using template B_1 maps is a promising strategy to reduce the acquisition time and analyze studies with no B_1 map acquired. This methodology reduces the cost of not using a subject-specific correction by increasing the accuracy of the computed T_1 values, which are comparable to the reference ones. That has a clear impact on the quantitative analyses carried out using these maps. In addition this method shows significant improvement with respect to the uncorrected maps and to the N3 corrected maps in terms of segmentation accuracy, which is important in the study of a considerable number of pathologies.

5. REFERENCES

[1] R.W. McCarley, C.G. Wible, et al., "MRI anatomy of schizophrenia", *Biol. Phsychiatry*, vol. 4, pp. 1099-1119, 1999.

[2] D. Kidron, S.E. Black, et al., "Quantitative MR volumetry in Alzheimer's disease", *Neurology*, vol. 49(6), pp. 1504-12, 1997.

[3] A.W.-C. Liew, and H. Yan, "Current methods in the automatic tissue segmentation of 3D magnetic resonance brain images", *Current Medical Imaging Reviews*, vol. 2, pp. 91-103, 2006.

[4] M. Bomans, K.H. Hohne, U. Tiede, et al., "3D segmentation of MR images of the head for 3D display", *IEEE-Trans. Med. Imaging*, vol. 9(2), pp. 177-183, 1990.

[5] T. McInerney, and D. Terzopoulos, "Deformable models in medical image analysis: A Review", *Medical Image Analysis*, vol. 1(2), pp. 91-108, 1996.

[6] N. Duta, and M. Sonka, "Segmentation and interpretation of MR brain images: An improved active shape model", *IEEE-Trans. Med. Imaging*, vol. 17(6), pp. 1049-1062, 1998.

[7] I.N. Manousakas, P.E. Undrill, G.G. Cameron, et al., "Split-and-merge segmentation of magnetic resonance medical images: Performance evaluation and extension to three dimensions", *Comput Biomed Res*, vol. 31(6), pp. 393-412, 1998.

[8] M. Joliot, and B.M. Mazoyer, "Automatic segmentation of head MRI images by knowledge guided thresholding", *Comput. Med. Imaging Graph.*, vol. 15(4), pp. 233-240, 1991.

[9] J.C. Rajapakse, J.N. Giedd, and J.L. Rapoport, "Statistical approach to segmentation of single-channel cerebral MR images", *IEEE-Trans. Med. Imag.*, vol. 16(2), pp. 176-186, 1997.

[10] J.C. Bezdek, *Pattern recognition with fuzzy objective function algorithms*, Plenum Press, New York, 1981.

[11] H. Wang, S. Riederer, and J. Lee, "Optimizing the precision in T1 relaxation estimation using limited flip angles," *Magn. Reson.Med.*, vol. 5, pp. 399-416, 1987.

[12] H.-L. M. Cheng and G. A. Wright, "Rapid high-resolution T1 mapping by variable flip angles: accurate and precise measurement in the presence of radiofrequency field inhomogeneity," *Magn. Reson. Med.*, vol. 55, pp. 566-574, 2006.

[13] J. M. Jin, J. Chen, W. C. Chew, et al. "Computation of electromagnetic fields for high-frequency magnetic resonance imaging applications," *Phys. Med. Biol.*, vol. 41, pp. 2719-2738, 1996.

[14] P.-F. Cheng, R.G. Steen, A. Yezzi, et al., "Joint brain parametric T1-map segmentation and RF inhomogeneity calibration", *Int. J. Biomed. Imag.*, vol. 2009, pp. 1-14, 2009.

[15] B. Belaroussi, J. Mille, S. Carme, et al., "Intensity non-uniformity correction in MRI: Existing methods and their validation," *Medical Image Analysis*, vol. 10, pp. 234-246, 2006.

[16] Z. Hou, "A Review on MR Image Intensity Inhomogeneity Correction," *Int J Biomed Imaging*, vol. 2006, pp. 1-11, 2006.

[17] J. G. Sled and A. P. Zijdenbos, "A Nonparametric Method for Automatic Correction of Intensity Nonuniformity in MRI Data," *IEEE-Trans. Med. Imaging*, vol. 17, pp. 87-97, 1998.

[18] Y. Ishimori, K. Yamada, H. Kimura, et al., "Correction of inhomogeneous RF field using multiple SPGR signals for high-field spin-echo MRI", *Magn.Reson.Med.Sci.*,vol.6,pp.67-73, 2007.

[19] R. Treier, A. Steingoetter, M. Fried, et al. "Optimized and combined T1 and B1 mapping technique for fast accurate T1 quantification in Constrast-Enhanced abdominal MRI," *Magn. Reson. Med.*, vol. 57, pp. 568-576, 2007.

[20] V. Yarnykh, "Actual flip-angle imaging in the pulsed steady state: A method for rapid 3D mapping of the transmitted RF field," *Magn. Reson. Med.*, vol. 57, pp. 192-200, 2007.

[21] S. C. L. Deoni, "High-resolution T1 mapping of the brain at 3T with driven equilibrium single pulse observation with T1 high-speed incorporation of RF field inhomogeneities (DESPOT1-HIFI)," *J. Magn. Reson. Imaging*, vol. 26, pp. 1106-1111, 2007.

[22] M.A. Castro, J. Yao, C. Lee, et. al, "T1 mapping with B1 field and motion correction in brain MRI images: Application to brain DCE-MRI," *MICCAI Proc. Workshop on analysis of Functional Medical Images*, New York, USA, 2008.

[23] S.C.L. Deoni, B.K. Rutt, and T.M. Peters, "Rapid Combined T1 and T2 Mapping Using Gradient Recalled Acquisition in the Steady State," *Magn. Reson. Med.*, vol. 49, pp. 515-526, 2003.

[24] S. Smith, "Fast robust automated brain extraction," *Hum. Brain Mapp.*, vol. 17, pp. 143-155, 2002.